Progress In Electromagnetics Research, Vol. 141, 79–98, 2013

FLUCTUATING TARGET DETECTION IN LOW-GRAZING ANGLE WITH MIMO RADAR

Jin Can Ding*, Hao Wen Chen, Xiang Li, and Zhao Wen Zhuang

Research Institute of Space Electronics Information Technology, Electronics Science and Engineering School, National University of Defense Technology, Changsha 410073, P. R. China

Abstract—This paper focuses on the fluctuating target detection in low-grazing angle using Multiple-input Multiple-output (MIMO) radar systems with widely separated antennas, where the multipath effects are very abundant. The performance of detection can be improved via utilizing the multipath echoes, which is equivalent to improve the signal-to-noise ratio (SNR) by using multipath echoes. First, the reflection coefficient considering the curved earth effect is derived. Then, the general signal model for MIMO radar is introduced for fluctuating target in low-grazing angle. Using the Neyman-Pearson sense, the detectors of fluctuating targets, i.e., Swerling 1–4, with multipath are analyzed. Finally, the simulation results show that the performance can be enhanced markedly when the multipath effects are considered.

1. INTRODUCTION

Over the last decade, the multiple-input multiple-output (MIMO) approach for radar processing has drawn a great deal of attention and has been applied to various radar scenarios and problems, where the term MIMO refers to the use of multiple-transmit as well as multiple-receive antennas. MIMO radar is categorized into two classes: the statistical MIMO radar and colocated MIMO radar, depending on their antenna placement [1–17]. The advantages of MIMO radar with colocated antennas have been studied extensively, which include improved detection performance and higher resolution [18], higher sensitivity or detection moving targets [19], and increased

Received 27 April 2013, Accepted 22 June 2013, Scheduled 12 July 2013
* Corresponding author: Jin Can Ding (jincanding@163.com).

degrees of freedom for transmission beamforming [20]. MIMO radar with widely separated antennas can capture the spatial diversity of the target's radar cross section (RCS) [21]. This spatial diversity provides radar systems with the ability to improve target parameter estimation [22, 23], high resolution target localization [24], and tracking performance [25].

Much published literature has concerned the issue of MIMO radar detection. Guan et al. [26] investigated the detection problem of the MIMO radar system with distributed apertures in Gaussian colored noise and partially correlated observation channels. Tang and Huang [27] introduced relative entropy as a measure to radar detection theory and analyzed the detection performance of MIMO radar and phased array radar. Tang et al. [28] investigated detection performance of MIMO radar for Rician target. In [29], the optimal detector in the Neyman-Pearson sense was derived for the statistical MIMO radar using orthogonal waveforms. Aittomaki et al. [30] applied the Swerling models to target detection and derived the optimal test statistics for a statistical MIMO radar using non-orthogonal signal. For low-grazing angle detection of MIMO radar, Jin et al. [31] utilized the time reversal technique in a multipath environment to achieve high target detectability of MIMO radar.

Low-grazing angle targets are difficult to detect, which is one of the great threats propelling radar development. Otherwise, detecting of low-altitude targets is of great significance to counter low-altitude air defense penetration. However, up to now, this problem has not been effectively resolved. Multipath effect plays an important role on the low-altitude target detection, by which the target echo signal is seriously polluted, even counteracted [32]. Two aspects can be considered for multipath: suppressing multipath and utilizing it. However, in a statistical sense, detection may be enhanced by the presence of multipath [33].

In this paper, we consider low-grazing angle fluctuating targets (Swerling 1–4) detection in multipath environment for MIMO radar. First of all, the reflecting coefficient is derived, considering the curved earth effect. Then, the general signal model for MIMO radar is introduced for fluctuating target in low-grazing angle. With the sense of Neyman-Pearson, the detectors of Swerling 1–4 are respectively derived. Via simulation analysis, we can find that the detection performance can be enhanced markedly when the multipath effects are considered. The main contributions of our paper are twofold: one is how to utilize multipath effects for MIMO radar in low-grazing angle; the other is to compare the detection performance with fluctuating target models.

2. MULTIPATH GEOMETRY MODEL

A point source at a distance of R_d from the receiver is considered. If the source is assumed to be a narrowband signal, it can be represented by

$$x(t) = ae^{j(\omega t+\phi)} \tag{1}$$

where a is the amplitude, ω the angular frequency, and ϕ the initial phase. In the presence of multipath, the received by the receiver consists of two components, namely, the direct and indirect signal. For a simple multipath model of a flat earth, the direct signal is given by

$$x_d(t) = x(t)e^{-j\kappa R_d} \tag{2}$$

And the indirect signal is

$$x_i(t) = x(t)\rho e^{j\phi}e^{-j\kappa R_i} \tag{3}$$

$$R_i = R_1 + R_2 \tag{4}$$

where $\rho e^{j\phi}$ is the complex reflection coefficient, $\kappa = 2\pi/\lambda$ the wave number, λ the wavelength, and R_i the total length of the indirect path. The target range R_d can be obtained from the time delay. Thus, the total received signal is given by

$$x_r(t) = x_d(t) + x_i(t) \tag{5}$$

To model the received signals more accurately, the curvature of the signal path due to refraction in the troposphere, in addition to the curvature of the earth itself, must be taken into account. The multipath geometry for a curved earth is given in Figure 1.

Firstly, obtain φ according to the law of cosine as

$$\varphi = \arccos\left(\frac{(h+R_e)^2 + (Z_k+R_e)^2 - R_d^2}{2\,(h+R_e)\,(Z_k+R_e)}\right) \tag{6}$$

where, $\arcsin(\cdot)$ stands for the arcsin$e$, and h and Z_k are the height of target and height of radar, respectively. R_e is the effective radius of the imaginary earth [34], given by

$$R_e = R_0\left(1 + 6.37\times 10^{-3}\frac{dU}{dh}\right)^{-1} \tag{7}$$

where U is called the radio refractivity.

The horizon distance is computed by $r = R_e\varphi$, and the distance from the radar to the point of reflection r_1 can be found by solving the following cubic equation as

$$2r_1^3 - 3rr_1^2 + \left[r^2 - 2R_e\,(Z_k+h)\right]r_1 + 2R_eZ_kr = 0 \tag{8}$$

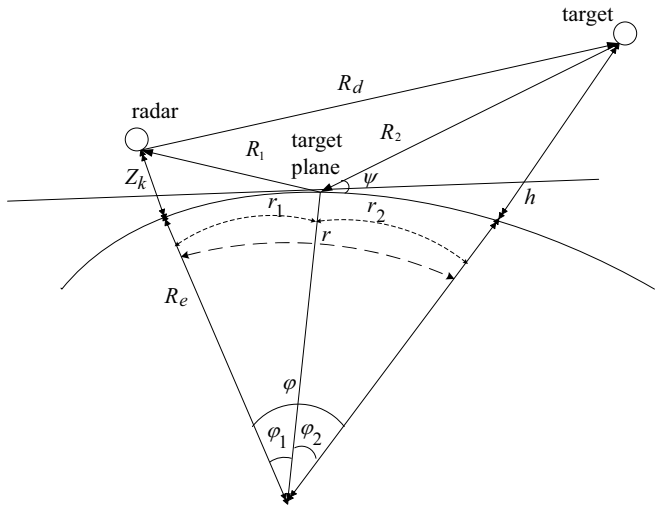

Figure 1. Multipath geometry for a curved earth.

Next, we solve φ_1, φ_2 using r_1 by

$$\varphi_1 = r_1/R_e \tag{9}$$

$$\varphi_2 = (r - r_1)/R_e \tag{10}$$

Using the law of cosine yields

$$R_1 = \sqrt{R_e^2 + (R_e + Z_k)^2 - 2R_e\,(R_e + Z_k)\cos\varphi_1} \tag{11}$$

$$R_2 = \sqrt{R_e^2 + (R_e + h)^2 - 2R_e\,(R_e + h)\cos\varphi_2} \tag{12}$$

$$R_d = \sqrt{(h+R_e)^2+(R_e+Z_k)^2-2(h+R_e)(R_e+Z_k)\cos(\varphi_1+\varphi_2)} \tag{13}$$

Then, the grazing angle ψ is

$$\psi = \pi/2 - 1/2\arccos\left(\frac{R_1^2 + R_2^2 - R_d^2}{2R_1R_2}\right) \tag{14}$$

The term $\rho e^{j\phi}$ in (3) generally consists of the Fresnel reflection coefficient, divided into the vertical polarization Γ_v and horizontal polarization Γ_h, the divergence factor D due to a curved surface, and the surface roughness factor ρ_s, i.e., $\rho e^{j\phi} = \Gamma_{(v,h)} D \rho_s$. The vertical polarization and horizontal polarization Fresnel reflection coefficients are respectively given by [32]

$$\Gamma_v \simeq \frac{\psi\sqrt{\varepsilon_c} - 1}{\psi\sqrt{\varepsilon_c} + 1} \tag{15}$$

$$\Gamma_h \simeq \frac{\psi - \sqrt{\varepsilon_c}}{\psi + \sqrt{\varepsilon_c}} \tag{16}$$

where ε_c is the complex dielectric constant, which is given by [34]

$$\varepsilon_c = \varepsilon/\varepsilon_0 - j60\lambda\sigma \tag{17}$$

$\varepsilon/\varepsilon_0$ is the relative dielectric constant of the reflecting medium, and σ is its conductivity. Thus, the Fresnel reflection coefficient is determined by the grazing angle under a deterministic condition [34].

$$D \simeq \left(1 + \frac{2r_1 r_2}{R_e r\psi}\right)^{-1/2} \tag{18}$$

The surface roughness factor ρ_s is given by [34]

$$\rho_s = e^{-\mu} \tag{19}$$

$$\mu = \begin{cases} 2[2\pi\eta]^2 & \eta \le 0.1\,\text{rad} \\ 0.16\eta^2 + 7.42\eta + 0.0468 & \text{otherwise} \end{cases} \tag{20}$$

and η is the surface roughness factor given by [34]

$$\eta = \frac{\sigma_H \psi}{\lambda} \tag{21}$$

where σ_H is the Root-Mean-Square (RMS) surface height irregularity. From (14)–(20), we can see that the specular reflection coefficient depends on the grazing angle. The other parameters can be obtained when a model is given, therefore, the specular reflection coefficient is a function of the grazing angle ψ, i.e., $f(\psi) = \rho e^{j\phi}$. Submitting (14)–(20) in $f(\psi) = \rho e^{j\phi}$ yields

$$\rho e^{j\phi} = \left(\frac{a_1 + b_1}{c_1} + j\frac{a_2 - b_2}{c_1}\right) \times \left(1 + \frac{2r_1 r_2}{R_e r\psi}\right)^{-1/2} e^{-\mu} \tag{22}$$

where

$$\begin{cases} a_1 = \left(\psi^2 k\cos\theta - 2\psi k^{\frac{1}{2}}\cos\frac{\theta}{2} + 1\right)\left(\psi^2 k\cos\theta - 1\right) \\ b_1 = \left(\psi^2 k\sin\theta - \psi k^{\frac{1}{2}}\sin\frac{\theta}{2}\right)\psi^2 k\sin\theta \\ a_2 = \psi^2 k\sin\theta\left(\psi^2 k\cos\theta - 2\psi k^{\frac{1}{2}}\cos\frac{\theta}{2} + 1\right) \\ b_2 = \left(\psi^2 k\cos\theta - 1\right)\left(\psi^2 k\sin\theta - \psi k^{\frac{1}{2}}\sin\frac{\theta}{2}\right) \\ c_1 = \left(\psi^2 k\cos\theta - 1\right)^2 + \psi^4 k^2\sin^2\theta \\ k = \sqrt{\left(\frac{\varepsilon}{\varepsilon_0}\right)^2 + (60\lambda\sigma)^2} \\ \theta = \arctan\frac{\varepsilon}{60\lambda\sigma\varepsilon_0} \end{cases} \tag{23}$$

thus, ρ is given by

$$\rho = \sqrt{\left(\frac{a_1 + b_1}{c_1}\right)^2 + \left(\frac{a_2 - b_2}{c_1}\right)^2} D\rho_s \tag{24}$$

It is worth to point out that the diffuse reflection component is treated as the incoherent white Gaussian noise, for simplicity [34]. Thus, the diffuse noise component can be combined with receiver noise as the effective noise term in signal model. Figure 2 shows that the reflection coefficient amplitude (ρ_s) surface and its contour varying with the antenna height and target height. From Figure 2(b), we can see that the reflection coefficient increases with the target height or the antenna height when both of them are smaller than 1000 m, otherwise, the reflection coefficient decreases, where the condition of low-grazing angle is not satisfied. This is due to the angle of reflection increases with the target and the antenna height increasing in (14).

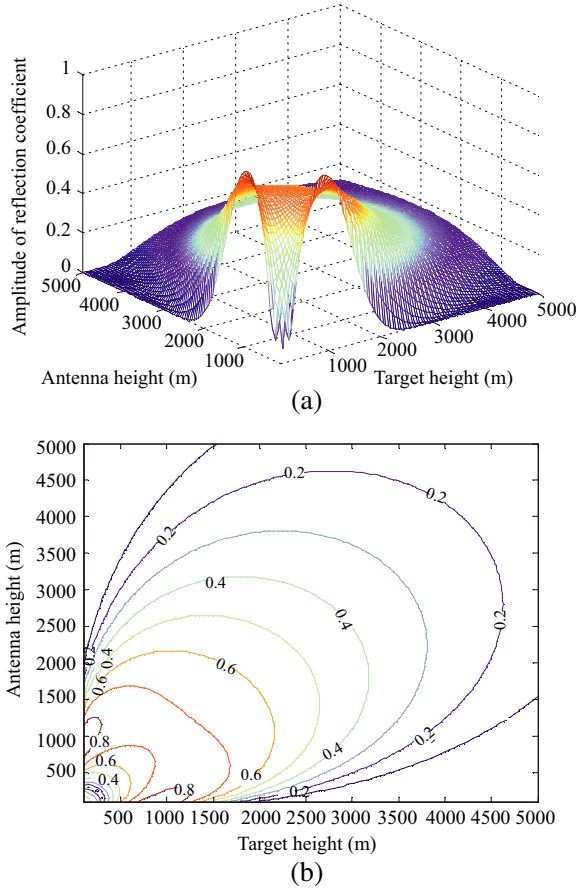

Figure 2. Reflection coefficient amplitude surface and its contour versus target and antenna height.

3. MIMO RADAR MULTIPATH SIGNAL

In this section, we consider the problem of detecting a stationary or slowly moving point target immersed in a multipath rich scattering environment.

For simplicity, assume that all antennas and targets are on the same plane, which can be easily extended to three-dimension (3-D). Consider a MIMO radar system with M_t transmit and M_r receive antennas. Assume the transmit antennas located at $T_k(x_{tk}, y_{tk})$, $k = 1, \ldots, M_t$ and the receive antennas located at $R_l(x_{rl}, y_{rl})$, $l = 1, \ldots, M_r$. The set of transmitted waveforms in lowpass equivalent form is $\sqrt{E/M_t}s_k(t)$, $k = 1, \ldots, M_t$, where $\int_T |s_k(t)|^2 = 1$, E is the total transmitted energy, and T is the waveforms' duration. Normalization by M_t makes the total energy independent of the number of transmitters. To achieve the orthogonality among the transmitted waveforms, we assume that $\int_T s_k(t)s_m^*(t-\tau)dt = 0$ for all $k \neq m$, where $\{\cdot\}^*$ is the complex conjugate operator.

In the presence of multipath, considering atmosphere refraction and the curved earth effect, the reflected radar signals from a point target include four part: directly-directly (dd), directly-reflected (dr), reflected-directly (rd), and reflected-reflected (rr) paths. Assume the point target located at $B(x_0, y_0)$ and reflected point in ground located at $P_i(x_i, y_i)$, $i = 1, 2$, as shown in Figure 3.

The received signal of MIMO radar with widely separated antennas is given by [2]

$$r_{dd}(t) = \sqrt{E/M_t}\delta_0 s_k(t)\exp[-j2\pi f_c(\tau_{tk}(T_k, B)+\tau_{rl}(R_l+B))]+e(t) \quad (25)$$

where δ_0 is the complex amplitude due to the target characteristics, f_c the carrier frequency, and $e(t)$ the Gaussian noise. The direct path delay $\tau_{tk}(T_{\rm k}, B)$ and $\tau_{rl}(R_l, B)$ are given as follows:

$$\tau_{tk}(T_k, B) = \frac{\sqrt{(x_{tk}-x_0)^2+(y_{tk}-y_0)^2}}{c} \quad (26)$$

$$\tau_{rl}(R_l, B) = \frac{\sqrt{(x_{rl}-x_0)^2+(y_{rl}-y_0)^2}}{c} \quad (27)$$

Similarly, we can get directly-reflected path echo signal as follows:

$$r_{dr}(t) = \sqrt{\frac{E}{M_t}}\zeta_1\delta_0 s_k(t)\, h_{kl}^{dr}+e(t) \quad (28)$$

where $h_{kl}^{dr} = \exp\left[-j2\pi f_c\left(\tau_{tk}\left(T_k, B\right)+\tau_0\left(B, P_2\right)+\tau_{rl}\left(P_2, R_l\right)\right)\right]$.

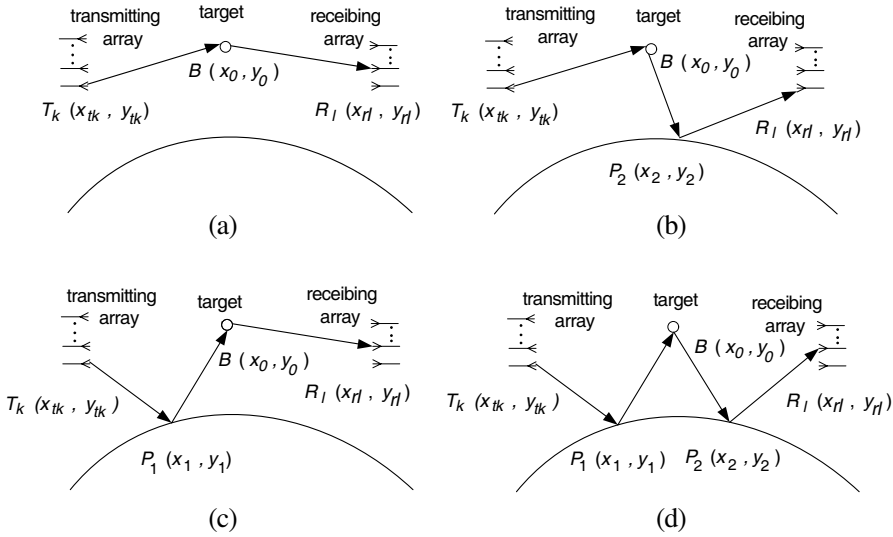

Figure 3. Multipath geometry for MIMO radar. (a) Directly-directly path, (b) directly-reflected path, (c) reflected-directly path, (d) reflected-directly path.

And the reflected-directly path echo signal as

$$r_{rd}(t) = \sqrt{\frac{E}{M_t}}\zeta_2\delta_0 s_k(t)\, h_{kl}^{rd} + e(t) \tag{29}$$

where $h_{kl}^{rd} = \exp\left[-j2\pi f_c\left(\tau_{tk}\left(T_k, P_1\right) + \tau_0\left(P_1, B\right) + \tau_{rl}\left(R_l, B\right)\right)\right]$.

The reflected-reflected path echo signal as

$$r_{rr}(t) = \sqrt{\frac{E}{M_t}}\zeta_3\delta_0 s_k(t)\, h_{kl}^{rr} + e(t) \tag{30}$$

where $h_{kl}^{rd} = \exp[-j2\pi f_c(\tau_{tk}(T_k, P_1) + \tau_0(P_1, B) + \tau_0(B, P_2) + \tau_{rl}(P_2, R_l))]$, $\zeta_i, i = 1, 2, 3$ is the reflect coefficient. Because the grazing angles are different, the reflect coefficients satisfy $\zeta_1 \neq \zeta_2 \neq \zeta_3$ and $\zeta_3 = \zeta_1\zeta_2$. The time delay $\tau_{tk}(T_k, P_1)$, $\tau_{rl}(P_2, R_l)$, $\tau_{tk}(P_1, B)$, $\tau_0(B, P_2)$ are respectively given by

$$\begin{cases} \tau_{tk}(T_k, P_1) = \dfrac{\sqrt{(x_{tk}-x_1)^2+(y_{tk}-y_1)^2}}{c} \\ \tau_{rl}(P_2, R_l) = \dfrac{\sqrt{(x_2-x_{rl})^2+(y_2-y_{rl})^2}}{c} \\ \tau_{tk}(P_1, B) = \dfrac{\sqrt{(x_1-x_0)^2+(y_1-y_0)^2}}{c} \\ \tau_0(B, P_2) = \dfrac{\sqrt{(x_0-x_2)^2+(y_0-y_2)^2}}{c} \end{cases} \tag{31}$$

The received signal of a pair of transmit-receive antennas is

$$r_{kl}(t) = r_{dd}(t) + r_{dr}(t) + r_{rd}(t) + r_{rr}(t) \tag{32}$$

The received signal for whole MIMO radar with multipath is

$$r(t) = \sum_{k=1}^{M_t} \sum_{l=1}^{M_r} r_{kl}(t) + e(t) \tag{33}$$

4. FLUCTUATING TARGET MULTIPATH DETECTOR OF MIMO RADAR

In this section, we analyze the detection performance, under the multipath environment with the different Swerling scattering models, for MIMO radar with widely separated antennas. The Swerling scattering model is commonly used in the radar community to model the distribution and the temporal correlation of the target RCS. The Swerling scattering model includes four different cases for modeling both slow and fast fluctuations of the RCS [35], i.e., Swerling 1, 2, 3 and 4.

We formulate the MIMO radar detection problem. As the following binary hypothesis test

$$\begin{cases} \mathrm{H}_0: & \text{no target exist} \\ \mathrm{H}_1: & \text{target exist} \end{cases} \tag{34}$$

Now we consider the fluctuating target base on white Gaussian noise environment of N samples noncoherent detection in low-grazing angle. Assume that target component amplitude and phase are unknown. Thus, the independent data sample $r_{kl}(n)$ is a complex constant which comprises of real amplitude $\tilde{m}_{kl}$ and phase θ_{kl}, $m_{kl} = \tilde{m}_{kl} \exp(j\theta_{kl})$. The data also contains white Gaussian noise e_{kl}. Without loss of generality, we assume that all noise power spectrum is β^2. Then, the data is given by [35]

$$r_{kl}(n) = m_{kl} + e_{kl} \tag{35}$$

where $\tilde{m}_{kl} = \alpha(1 + \rho_{kl}^{(dr)} + \rho_{kl}^{(rd)} + \rho_{kl}^{(rr)})$, α is the amplitude due to the target characteristics, and $\rho_{kl}^{(\cdot)}$ are the amplitude of reflection coefficients of $k-l$th antenna pair.

Notice the noncoherent nature of the MIMO radar detector. Assume that one pair of antennas have N dimensional vector $\mathbf{z}$, thus, in MIMO radar system we can get a $G = M_t M_r N$ dimensional vector, i.e., $\mathbf{Z} = [\mathbf{z}_1, \ldots, \mathbf{z}_{M_t M_r}] = [z_{11}(1), \ldots, z_{11}(n), z_{21}(1), \ldots, z_{21}(n), \ldots, z_{kl}(n), \ldots,$

$z_{M_tM_r}(1),\ldots,z_{M_tM_r}(n)]$, $k=1,\ldots,M_t$, $l=1,\ldots M_r$, $n=1,\ldots,N$. The joint probability density function is [35]

$$p_{\mathbf{Z}}(\mathbf{Z}|\,\mathrm{H}_0)=\prod_{k=1}^{M_t}\prod_{l=1}^{M_r}\prod_{n=1}^{N}\frac{2z_{kl}(n)}{\beta^2}e^{-z_{kl}^2(n)/\beta^2} \tag{36}$$

$$p_{\mathbf{Z}}(\mathbf{Z}|\,\mathrm{H}_1)=\prod_{k=1}^{M_t}\prod_{l=1}^{M_r}\prod_{n=1}^{N}\frac{2z_{kl}(n)}{\beta^2}\,e^{-\left(z_{kl}^2(n)+\tilde{m}_{kl}^2\right)\Big/\beta^2}I_0\left(\frac{2\tilde{m}_{kl}z_{kl}(n)}{\beta^2}\right) \tag{37}$$

where $I_0(\cdot)$ is Bessel function, and it's likelihood ratio test (LRT) and logarithm LRT are respectively given by

$$\Lambda_{\mathrm{MIMO}}=\prod_{k=1}^{M_t}\prod_{l=1}^{M_r}\prod_{n=1}^{N}e^{-\tilde{m}_{kl}^2/\beta^2}I_0\left(\frac{2\tilde{m}_{kl}z_{kl}(n)}{\beta^2}\right)\ \begin{matrix}>\mathrm{H}_1\\<\mathrm{H}_0\end{matrix}\ \gamma \tag{38}$$

$$\ln\Lambda_{\mathrm{MIMO}}=\sum_{k=1}^{M_t}\sum_{l=1}^{M_r}\sum_{n=1}^{N}\left\{-\frac{\tilde{m}_{kl}^2}{\beta^2}+\ln\left[I_0\left(\frac{2\tilde{m}_{kl}z_{kl}(n)}{\beta^2}\right)\right]\right\}\ \begin{matrix}>\mathrm{H}_1\\<\mathrm{H}_0\end{matrix}\ \ln\gamma \tag{39}$$

(38) can be simplified as

$$\sum_{k=1}^{M_t}\sum_{l=1}^{M_r}\sum_{n=1}^{N}\ln\left[I_0\left(\frac{2\tilde{m}_{kl}z_{kl}(n)}{\beta^2}\right)\right]\ \begin{matrix}>\mathrm{H}_1\\<\mathrm{H}_0\end{matrix}\ \ln\gamma+\frac{\tilde{m}_{kl}^2}{\beta^2}=\mathrm{T}' \tag{40}$$

where, depending on the nature of the Bessel function, (39) can be further simplified as

$$\mathbf{z}'=\sum_{k=1}^{M_t}\sum_{l=1}^{M_r}\sum_{n=1}^{N}z_{kl}^2(n)\ \begin{matrix}>\mathrm{H}_1\\<\mathrm{H}_0\end{matrix}\ \frac{\mathrm{T}'\beta^4}{\tilde{m}^2} \tag{41}$$

where $\tilde{m}^2=N\sum_{k=1}^{M_t}\sum_{l=1}^{M_r}\tilde{m}_{kl}^2$, and (35) demonstrates that z' is the sufficient statistic.

In H_0, the Characteristic Function (CF) of $\mathbf{z}'$ is given by [35]

$$C_{\mathbf{z}'}(q;G)=\prod_{k=1}^{M_t}\prod_{l=1}^{M_r}\left(\frac{1}{1-jq}\right)^{klN} \tag{42}$$

while in H_1, the CF of $\mathbf{z}'$ is given by

$$C_{\mathbf{z}'}(q)=\prod_{k=1}^{M_t}\prod_{l=1}^{M_r}\left(\frac{1}{q+1}\right)^{klN}e^{-klN\sigma[q/1+q]} \tag{43}$$

where $\sigma=\tilde{m}^2\big/\beta^2$ is the signal-to-noise ratio (SNR).

For Swerling 1, the CF in H_1 and H_0 are respectively are given by [35]

$$C_{\mathbf{z}'}(q;\sigma,G) = \prod_{k=1}^{M_t}\prod_{l=1}^{M_r}\left(\frac{1}{q+1}\right)^{klN} e^{-klN\sigma[q/(q+1)]} \tag{44}$$

$$C_{\mathbf{z}'}(q;G) = \prod_{k=1}^{M_t}\prod_{l=1}^{M_r}\left(\frac{1}{1-jq}\right)^{klN} \tag{45}$$

The expectations of the target CF can be extracted from the RCS (also is the SNR), which is given by

$$\overline{C}_{\mathbf{z}'-\text{swerling1}}(q;\overline{\sigma},G) = \int_0^\infty p_\sigma(\sigma)\, C_{\mathbf{z}'}(q;\sigma,G) \tag{46}$$

where $p_\sigma(\sigma)$ is the SNR probability density function (PDF) and $\bar{\sigma}$ the mean of the SNR.

For Swerling 1, the distribution of SNR's PDF satisfies the following exponential distribution

$$p_\sigma(\sigma) = \frac{1}{\bar{\sigma}} e^{-\sigma/\bar{\sigma}} \tag{47}$$

Plugging (47) and (44) into (46), we can get the average CF of signal fluctuation as

$$\overline{C}_{\mathbf{z}'-\text{swerling1}}(q;\overline{\sigma},G) = \prod_{k=1}^{M_t}\prod_{l=1}^{M_r}\frac{1}{(1+q)^{klN-1}\left[1+q(1+klN\overline{\sigma})\right]} \tag{48}$$

for the hypothesis H_1, the PDF can be calculated by Fourier transformation as [35]

$$\begin{aligned} p_{\mathbf{z}'}\left(\mathbf{z}'|\mathrm{H}_1\right) &= \frac{1}{2\pi}\int_{-\infty}^{\infty}\overline{C}_{\mathbf{z}'}(q;\bar{\sigma},G)e^{-jq\mathbf{z}'}dq = \frac{1}{G\bar{\sigma}}\left(1+\frac{1}{G\bar{\sigma}}\right)^{G-2} \\ &\quad \times I\left[\frac{\mathbf{z}'}{(1+1/G\bar{\sigma})\sqrt{G-1}}, G-2\right] e^{-\mathbf{z}'/(1+G\bar{\sigma})} \end{aligned} \tag{49}$$

The detection probability of the Swerling 1 is given by

$$\begin{aligned} P_{D1} &= \int_\Gamma^\infty p_{\mathbf{z}'}\left(\mathbf{z}'|\mathrm{H}_1\right)d\mathbf{z}' \\ &= \int_\Gamma^\infty \frac{1}{G\bar{\sigma}}\left(1+\frac{1}{G\bar{\sigma}}\right)^{G-2} I\left[\frac{\mathbf{z}'}{(1+1/G\bar{\sigma})\sqrt{G-1}}, G-2\right]e^{-\mathbf{z}'/(1+G\bar{\sigma})}d\mathbf{z}' \\ &= \left(1+\frac{1}{G\bar{\sigma}}\right) \end{aligned} \tag{50}$$

where Γ is the threshold.

In H_0, the PDF of $\mathbf{z}'$ is given by

$$P_{\mathbf{z}'}\left(\mathbf{z}'|\mathrm{H}_0\right) = \frac{\left(\mathbf{z}'\right)^{G-1}}{(G-1)!}e^{-\mathbf{z}'} \tag{51}$$

while the false alarm probability of $\mathbf{z}'$ is given by

$$P_{FA} = \int_{\mathrm{T}}^{\infty} \frac{\left(\mathbf{z}'\right)^{G-1}}{(G-1)!}e^{-\mathbf{z}'}dz' = 1 - I\left(\frac{\Gamma}{\sqrt{G}}, G-1\right) \tag{52}$$

From (52), the false alarm probability depends only on the threshold and number of sampling. Thus, for four Swerling models, if the threshold is given, the false alarm probabilities of different Swerling models are equal to each other.

For Swerling 2, the received signals are uncorrelated among different pluses, and the SNR at each sampling points are different. Then the CF of z' is given by

$$\begin{aligned}\bar{C}_{\mathbf{z}'-\mathrm{swerling2}}(q;\bar{\sigma},G) &= \left[\frac{1}{1+q}\int_0^{\infty} P_\sigma(\sigma)e^{-\sigma\left(\frac{q}{1+q}\right)}d\sigma\right]^G \\ &= \frac{1}{\left[1+q\left(1+\bar{\sigma}\right)\right]^G}\end{aligned} \tag{53}$$

The PDF of SNR in Swerling 2 is the same as the one of Swerling 1. Thus, the PDF of $\mathbf{z}'$, under the hypothesis H_1, is given by

$$\begin{aligned}P_{\mathbf{z}'}\left(\mathbf{z}'|\mathrm{H}_1\right) &= \frac{1}{2\pi}\int_{-\infty}^{\infty}\overline{C}_{\mathbf{z}'}(q;\bar{\sigma},G)e^{-jq\mathbf{z}'}dq \\ &= \frac{\mathbf{z}'^{G-1}e^{-\mathbf{z}'/1+\bar{\sigma}}}{\left(1+\bar{\sigma}\right)^G(G-1)!}\end{aligned} \tag{54}$$

the detection probability of the Swerling 2 is

$$\begin{aligned}P_{D2} &= \int_{\Gamma}^{\infty} p_{\mathbf{z}'}\left(\mathbf{z}'|\mathrm{H}_1\right)d\mathbf{z}' = \int_{\Gamma}^{\infty}\frac{\mathbf{z}'^{G-1}e^{-\mathbf{z}'/(1+\bar{\sigma})}}{\left(1+\bar{\sigma}\right)^G(G-1)!}d\mathbf{z}' \\ &= 1 - I\left(\frac{\Gamma}{\left(1+\bar{\sigma}\right)\sqrt{G}}, G-1\right)\end{aligned} \tag{55}$$

For Swerling 3, we can use a similar process to Swerling 1. Thus, the PDF of SNR distributed as chi-square distribution is given by

$$P_\sigma(\sigma) = \frac{4\sigma}{\bar{\sigma}}e^{-2\sigma/\bar{\sigma}} \tag{56}$$

and the CF is

$$\begin{aligned}\bar{C}_{\mathbf{z}'-\text{swerling3}}(q;\bar{\sigma},G) &= \int_0^{\infty} P_{\sigma}(\sigma)C_{\mathbf{z}'}(q;\sigma,G)d\sigma \\ &= \frac{(q+1)^G}{\left[(1+\bar{\sigma})\,q+1\right]^{2G}} \end{aligned} \tag{57}$$

Thus, under the hypothesis H_1, the PDF of $\mathbf{z}'$ is given by

$$\begin{aligned}P_{\mathbf{z}'}\left(\mathbf{z}'|\mathrm{H}_1\right) &= \frac{1}{2\pi}\int_{-\infty}^{\infty}\overline{C}_{\mathbf{z}'}(q;\bar{\sigma},G)e^{-jq\mathbf{z}'}dq \\ &= \frac{1}{G\bar{\sigma}}\left(1+\frac{2}{G\bar{\sigma}}\right)^{G-2} \\ &\quad \times I\left(1+\frac{\mathbf{z}'}{1+(G\overline{\sigma}/2)}-\frac{2(G-2)}{G\bar{\sigma}},G-2\right)e^{-\mathbf{z}'/(1+G\bar{\sigma}/2)}\end{aligned} \tag{58}$$

The detection probability of the Swerling 3 is

$$\begin{aligned}P_{D3} &= \int_{\Gamma}^{\infty} p_{\mathbf{z}'}\left(\mathbf{z}'|\mathrm{H}_1\right)d\mathbf{z}' \\ &= \left(1+\frac{2}{G\bar{\sigma}}\right)^{G-2}\left(1+\frac{\Gamma}{1+(G\bar{\sigma}/2)}-\frac{2\,(G-2)}{G\bar{\sigma}}\right) \\ &\quad \times e^{-\Gamma/(1+G\bar{\sigma}/2)}\end{aligned} \tag{59}$$

For Swerling 4, we can use a similar process to Swerling 2. Thus, the PDF of SNR is described as chi-square distribution, being same as (56). The detection probability is given by

$$\begin{aligned}P_{D4} &= c^G\sum_{k=0}^{G}\frac{G!}{k!\,(G-k)!}\left(\frac{1-c}{c}\right)^{G-k} \\ &\quad \times\left[\sum_{l=0}^{2G-k-1}\frac{e^{-c\mathrm{T}}\,(c\Gamma)^l}{l!}\right]\end{aligned} \tag{60}$$

where $c = 1/1+(\bar{\sigma}/2)$.

5. NUMERICAL SIMULATIONS

In this section, we consider several numerical examples that compare the performance of detection for different Swearling models with or without considering multipath effects. In our first example, we consider MIMO radar with three receive antennas and two transmit antennas. The transmit array is fixed at 10 m, 80 m, the receive array fixed at 100 m, 200 m, 300 m, the target's height fixed at 300 m, the range to

target fixed at 13 km, the radar frequency 2 GHz, and the dielectric constant 0.5. According to the heights of antennas (10 m, 80 m, 100 m, 200 m and 300 m), the surface roughnesses can be computed as 0.55, 0.33, 0.31, 0.27 and 0.26. We assume that the noise is Gaussian distribution. We consider the performance of the detection for MIMO radar in different probability of false alarm.

Figure 4 depicts the detection probability for Swerling 1–4 targets using the square-law detectors, with and without considering multipath effects, respectively, as a function of the SNR. The probability of false alarm is fixed at $P_{FA} = 10^{-5}$, 10^{-6}, 10^{-7}, and 10^{-8}, respectively. For the same SNR and false alarm, we can see that the detection

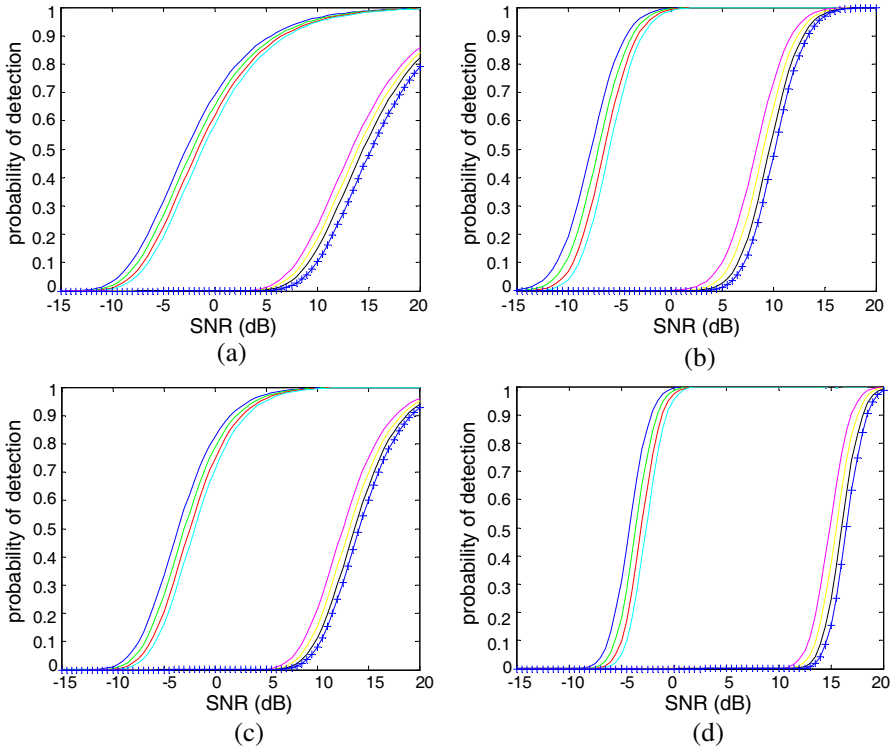

Figure 4. Detection performance for Swerling models, (a) Swerling 1, (b) Swerling 2, (c) Swerling 3, (d) Swerling 4, $P_{FA} = 10^{-5}$ multipath (blue curve), $P_{FA} = 10^{-6}$ multipath (green curve), $P_{FA} = 10^{-7}$ multipath (red curve), $P_{FA} = 10^{-8}$ multipath (cyan curve), $P_{FA} = 10^{-5}$ non-multipath (magenta curve), $P_{FA} = 10^{-6}$ non-multipath (yellow curve), $P_{FA} = 10^{-7}$ non-multipath (black curve), $P_{FA} = 10^{-8}$ non-multipath (+ curve).

performance with multipath respectively outperforms the one without considering multipath effect for all target cases. This is due to that using the multipath effects can improve the SNR.

Figure 5 depicts the performance comparison of four Swerling scatter models with and without multipath effect, respectively, where the probability of false alarm is set at $P_{FA} = 10^{-5}$. Form Figure 5, we can see that the detection performance of Swerling 2 outperforms the ones of the other targets models. This is due to the heavier tail of the probability density function of the Swerling 2 [35]. In the case without considering multipath effects, the SNR should be more than 10 dB to detect targets.

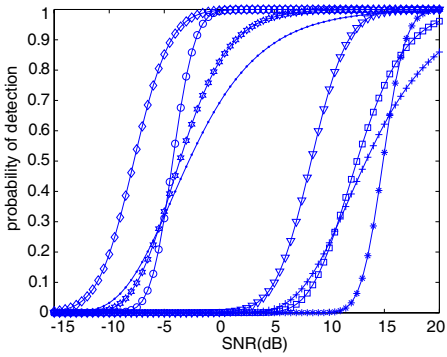

Figure 5. Comparison of four Swerling models, Swerling 1 multipath ($\cdot$ curve), Swerling 2 multipath ($\diamond$ curve), Swerling 3 multipath ($\star$ curve), Swerling 4 multipath ($\circ$ curve), Swerling 1 non-multipath ($+$ curve), Swerling 2 non-multipath (∇ curve), Swerling 3 non-multipath ($\square$ curve), Swerling 4 non-multipath ($*$ curve).

Table 1. Requirement of SNR (dB) for $P_D = 80\%$.

(a) Swerling 1

NA	2	3	4
SNR-M	7.15	1.48	−2.34
SNR-N	26.44	20.45	18.65

(b) Swerling 2

NA	2	3	4
SNR-M	4.98	−4.96	−11.13
SNR-N	19.98	13.64	9.87

(c) Swerling 3

NA	2	3	4
SNR-M	4.67	−0.93	−4.89
SNR-N	20.13	17.59	8.78

(d) Swerling 4

NA	2	3	4
SNR-M	4.14	−3.44	−7.16
SNR-N	10.12	9.74	8.78

NA: Number of antennas; SNR-M: SNR of multipath; SNR-N: SNR of no-multipath.

Figure 6 depicts the detection probability of four Swerling scatter models with different antenna numbers, as a function of SNR. The probability of false alarm is set at $P_{FA} = 10^{-6}$. We can see that with higher number of transmit antennas, receive antennas obtain the better detection performance. For the convenience of comparison, the requirements of SNR for $P_D = 80\%$ are shown in Table 1, according to Figure 6. This improvement of detection results from the spatial diversity gain.

To take the target height into account, Figure 7 depicts the detection performance of Swerling 1–4 models with target height, respectively. The heights of target are fixed at 200 m, 400 m, 600 m and the probabilities of false alarm fixed at $P_{fa} = 10^{-4}$. Figure 7 shows that the detection performance varies with the height of target.

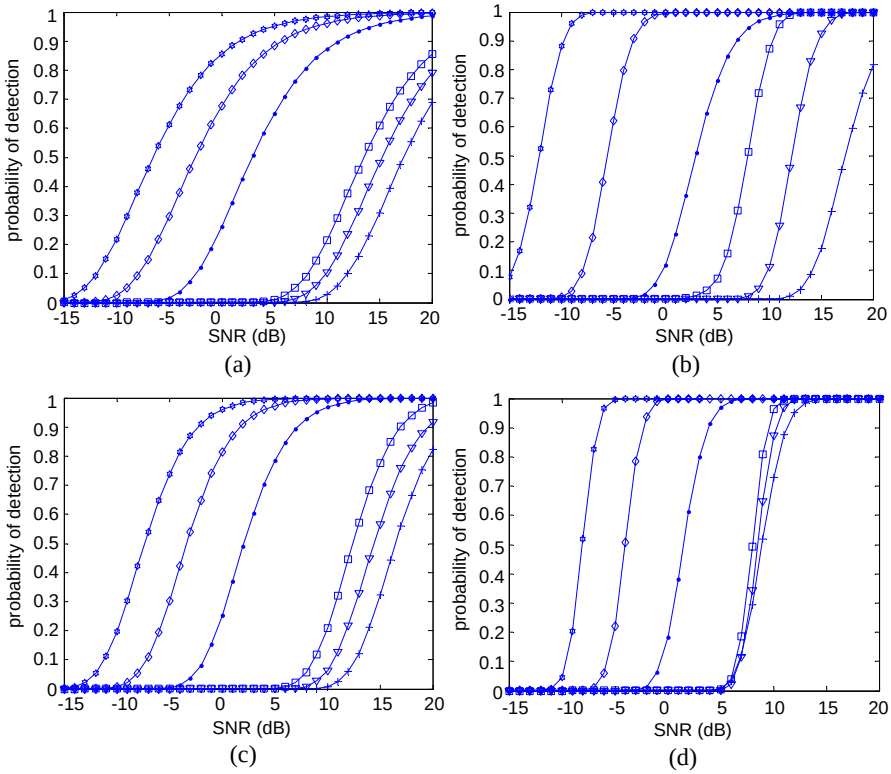

Figure 6. Detection performance of Swerling models with different number antennas, (a) Swerling 1, (b) Swerling 2, (c) Swerling 3, (d) Swerling 4, 2×2 multipath ($\cdot$ curve), 3×3 multipath ($\diamond$ curve), 4×4 multipath ($\star$ curve), 2×2 non-multipath ($+$ curve), 3×3 non-multipath (∇ curve), 4×4 non-multipath ($\square$ curve).

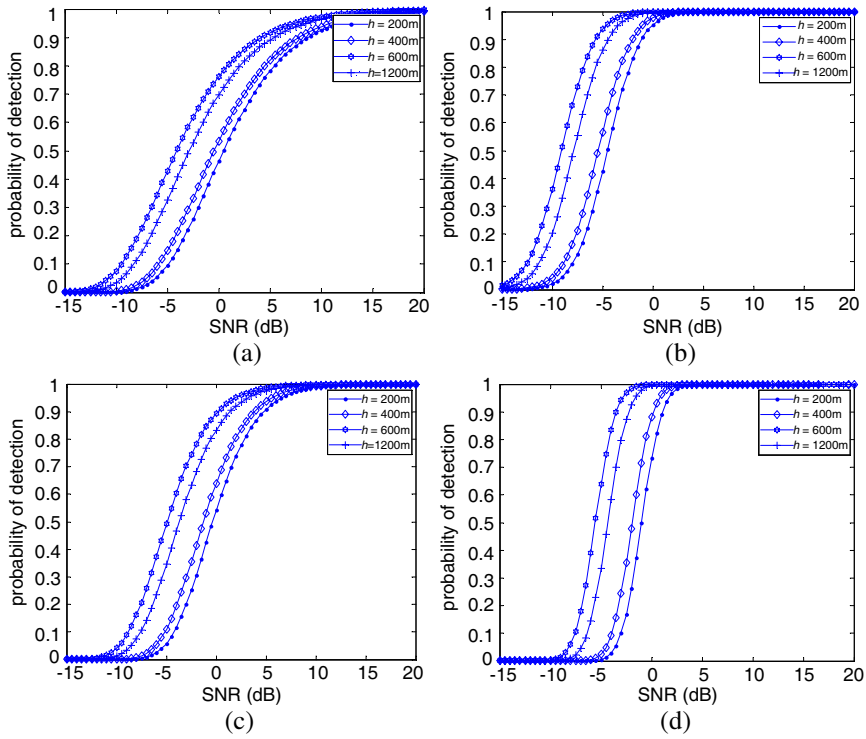

Figure 7. Detection performance of Swerling models varies with the height of target, (a) Swerling 1, (b) Swerling 2, (c) Swerling 3, (d) Swerling 4.

Furthermore, when the height of target increases attaining 1200 m, the multipath effects decrease, which validates the results in Figure 2.

6. CONCLUSIONS

In this paper, we introduce the concept of reflection coefficient under considering curved earth effect, and introduce the general signal model for MIMO radar in low-grazing angle, also compare the probabilities of detection of fluctuating targets with multipath and without multipath effects. The simulation results have demonstrated that with higher number of transmit antennas, receive antennas have higher probability of detection for all of the Swerling scatter models. Furthermore, the results of simulation have shown the importance of multipath effects for target detection in low-grazing angle. The target detection considering clutter in low-grazing angle will be considered for MIMO radar in the near future.

ACKNOWLEDGMENT

This research is funded in part by the National Natural Science Foundation of China under No. 60872134 and No. 60402032.

REFERENCES

1. Li, J. and P. Stoica, "MIMO radar with colocated antennas: Review of some recent work," *IEEE Signal Process. Mag.*, Vol. 24, No. 5, 106–114, Sep. 2007.
2. Haimovich, A. M., R. S. Blum, and L. Cimini, "MIMO radar with widely separated antennas," *IEEE Signal Process. Mag.*, Vol. 25, No. 1, 116–129, Jan. 2008.
3. Qu, Y., G. Liao, S. Q. Zhu, X. Y. Liu, and H. Jiang, "Performance analysis of beamforming for MIMO radar," *Progress In Electromagnetics Research*, Vol. 84, 123–134, 2008.
4. Yang, M. and G. Zhang, "Compressive sensing based parameter estimation for monostatic MIMO noise radar," *Progress In Electromagnetics Research Letters*, Vol. 30, 133–143, 2012.
5. Zhou, W., J. T. Wang, H. W. Chen, and X. Li, "Signal model and moving target detection based on MIMO synthetic aperture radar," *Progress In Electromagnetics Research*, Vol. 131, 311–329, 2012.
6. Bencheikh, M. L. and Y. Wang, "Combined esprit-rootmusic for DOA-DOD estimation in polarimetric bistatic MIMO radar," *Progress In Electromagnetics Research Letters*, Vol. 22, 109–117, 2011.
7. Hatam, M., A. Sheikhi, and M. A. Masnadi-Shirazi, "Target detection in pulse-train MIMO radar applying ICA algorithms," *Progress In Electromagnetics Research*, Vol. 122, 413–435, 2012.
8. Chen, J., Z. Li, and C.-S. Li, "A novel strategy for topside ionosphere sounder based on spaceborne MIMO radar with FDCD," *Progress In Electromagnetics Research*, Vol. 116, 381–393, 2011.
9. Huang, Y., P. V. Brennan, D. Patrick, I. Weller, P. Roberts, and K. Hughes, "FMCW based MIMO imaging radar for maritime navigation," *Progress In Electromagnetics Research*, Vol. 115, 327–342, 2011.
10. Ding, J. C., H. W. Chen, H. Q. Wang, X. Li, and Z. W. Zhuang, "Low-grazing angle target detection and system configuration of MIMO radar," *Progress In Electromagnetics Research B*, Vol. 48, 23–42, 2013.

11. Yang, M. and G. Zhang, "Parameter identifiability of monostatic MIMO chaotic radar using compressed sensing," *Progress In Electromagnetics Research B*, Vol. 44, 367–382, 2012.
12. Chen, H. W., J. C. Ding, X. Li, and Z. W. Zhuang, "MIMO radar systems design based on maximum channel capacity," *Progress In Electromagnetics Research B*, Vol. 34, 313–326, 2011.
13. Chen, H. W., X. Li, J. Yang, W. Zhou, and Z. W. Zhuang, "Effects of geometry configurations on ambiguity properties for bistatic MIMO radar," *Progress In Electromagnetics Research B*, Vol. 30, 117–133, 2011.
14. Le Marshall, N. W. D. and A. Z. Tirkel, "MIMO radar array for termite detection and imaging," *Progress In Electromagnetics Research B*, Vol. 28, 75–94, 2011.
15. Wang, G. and Y. L. Lu, "Sparse frequency waveform design for MIMO radar," *Progress In Electromagnetics Research B*, Vol. 20, 19–32, 2010.
16. Zhang, X., X. Gao, G. Feng, and D. Xu, "Blind joint DOA and DOD estimation and identifiability results for MIMO radar with different transmit/receive array manifolds," *Progress In Electromagnetics Research B*, Vol. 18, 101–119, 2009.
17. Sinha, N. B., R. N. Bera, and M. Mitra, "Digital array MIMO radar and its performance analysis," *Progress In Electromagnetics Research C*, Vol. 4, 25–41, 2008.
18. Bekkerman, I. and J. Tabrikian, "Target detection and localization using MIMO radars and sonars," *IEEE Trans. Signal Process.*, Vol. 54, No. 10, 3873–3883, Oct. 2006.
19. Forsythe, K., D. Bliss, and G. Fawcett, "Multiple-input multiple-output (MIMO) radar: Performance issues," *38th Asilomar Conference on Signals, Systems and Computers*, Vol. 1, 310–359, Pacific Grove, CA, Nov. 2004.
20. Stocia, P., J. Li, and Y. Xie, "On probing signal design for MIMO radar," *IEEE Trans. Signal Process.*, Vol. 55, No. 8, 4151–4161, Aug. 2007.
21. Li, J. and P. Stoica, *MIMO Radar Signal Processing*, Wiley-IEEE Press, New York, Oct. 2008.
22. He, Q., R. Blum, H. Godrich, and A. Haimovich, "Target velocity estimation and antenna placement for MIMO radar with widely separated antennas," *IEEE Journal of Selected Topics in Signal Processing*, Vol. 4, No. 1, 79–100, Feb. 2010.
23. Chen, H. W., Y. P. Chen, X. Li, and Z. W. Zhuang, "Extended ambiguity function for bistatic MIMO radar," *Journal of Systems*

Engineering and Electronics., Vol. 23, No. 2, 109–114, 2012.

24. Lehmann, N., A. Haimovich, R. Blum, and L. Cimini, "High resolution capabilities of MIMO radar," *40th Asilomar Conference on Signals, Systems and Computers*, 25–30, Pacific Groove, CA, Nov. 2006.
25. Godrich, H., V. Chiriac, A. Haimovich, and R. Blum, "Target tracking in MIMO radar systems: Techniques and performance analysis," *Proc. IEEE Radar Conf.*, 1111–1116, May 2010.
26. Guan, J. and Y. Huang, "Detection performance analysis for MIMO radar with distributed apertures in Gaussian colored noise," *Sci. China Ser. F: Inf. Sci.*, Vol. 52, No. 9, 1688–1696, 2009.
27. Tang, J., Y. Wu, Y. N. Peng, and X. T. Wang, "On detection performance and system configuration of MIMO radar," *Sci. China Ser. F: Inf. Sci.*, Vol. 52, No. 7, 1250–1257, 2009.
28. Tang, J., Y. Wu, Y. N. Peng, and X. T. Wang, "On detection performance of MIMO radar for Rician target," *Sci. China Ser. F: Inf. Sci.*, Vol. 52, No. 8, 1456–1465, 2009.
29. Fishler, E., A. Haimovich, and R. Blum, "Spatial diversity in radars-models and detection performance," *IEEE Trans. Signal Process.*, Vol. 54, No. 3, 823–838, Mar. 2006.
30. Aittomaki, T. and V. Koivunen, "Performance of MIMO radar with angular diversity under swerling scattering models," *IEEE Journal of Selected Topics in Signal Processing*, Vol. 4, No. 1, 101–114, Feb. 2010.
31. Jin, Y., J. M. F Moura, and N. O'Donoughue, "Time reversal in multiple-input multiple-output radar," *IEEE Journal of Selected Topics in Signal Processing*, Vol. 4, No. 1, 210–225, Feb. 2010.
32. Barton, D. K., "Low angle tracking," *IEEE Proceeding*, Vol. 62, No. 6, 687–704, Jun. 1974.
33. Silon, S. L. and B. D. Carlson, "Radar detection in multipath," *IEE Proceedings — Radar, Sonar, Navigation*, Vol. 146, No. 1, 45–54, Feb. 1999.
34. Lo, T. and J. Litva, "Use of a highly deterministic multipath signal model in low-angle tracking," *IEE Proceedings F — Radar and Signal Processing*, Vol. 138, No. 2, 163–171, Feb. 1991.
35. Richards, M. A., *Fundamentals of Radar Signal Processing*, McGraw-Hill, New York, 2005.